MICROSTRUCTURAL INVESTIGATION OF STRESS-DEPENDENT PERMEABILITY IN TIGHT OIL ROCKS

Hubert King, Michael Sansone, Pavel Kortunov, Ye Xu, Nicole Callen[1]
Shreerang Chhatre, Hemant Sahoo, Antonio Buono[2]

[1] ExxonMobil Research & Engineering Company
[2] ExxonMobil Upstream Research Company

This paper was prepared for presentation at the International Symposium of the Society of Core Analysts held in Vienna, Austria, 27 August – 1 September 2017.

1. ABSTRACT

Recent studies on several core-plug scale samples from tight oil reservoirs have demonstrated that such rocks can exhibit a significant, irreversible permeability decline with increase in net confining stress. Because this effect closely follows the expected stress change during drawdown in the field, the origins of this phenomena as well as a method to predict the magnitude relative to different rock types is valuable information for reservoir management. To better understand this effect, we have undertaken a series of in situ studies that demonstrate how an external stress field translates to microscopic strain at the pore scale and couples to the fluid transport. These studies rely on the coordinated use of low-field Nuclear Magnetic Resonance (NMR) and X-ray Micro-tomography (XMT). Making use of labeled fluids to enhance contrast, we are able to directly resolve how local strains affect fluid transport throughout the core plug. In a similar manner, proton NMR resolves how stress couples to deformation of the various pore systems, affecting the fluid content and their dynamics. Together, these techniques indicate that internal, high-permeability pathways play an important role in the stress dependence. Matrix permeability is much less affected. These higher-permeability zones are not ubiquitous in tight-oil rocks. Characterizing these zones and relating them to mineralogy and rock fabric is an attractive pathway to greater predictability for stress-dependent permeability for reservoir rock types.

2. INTRODUCTION

Over the last few years, technological advances including horizontal drilling and hydraulic fracturing have enabled production of vast amounts of oil and natural gas from shale and tight rocks. Most of the hydrocarbon production from tight rocks is carried out via primary depletion, where rock and fluid expansion provide the necessary driving force. Due to the low permeability of the rock matrix, large changes in pore pressure are expected for regions close to propped hydraulic fractures during hydrocarbon production. While the pore pressure is expected to change significantly, the overburden pressure is expected to be largely invariant during production timescale. As a result, the net confining stress (NCS = overburden pressure – pore pressure) experienced by near-fracture region of the rock matrix is expected to change significantly.

Changes in NCS can alter the permeability for unfractured rocks, matrix for tight/shales, and natural fractures. It can also affect hydraulic fractures, both propped and un-propped. Impairment of flow properties were found to be a function of the magnitude of pressure drawdown and the pressure history (hysteresis) [1-4]. Deterioration of the flow capability of the near-frac region alters the expected drainage area around fractures. Therefore, pressure dependent rock properties could provide key inputs for reservoir development business decisions in terms of well spacing, frac stage spacing, draw-down rates etc.

3. SAMPLES

This work is focused on samples from the productive *Wolfcamp* formation in the Midland Basin in West Texas. However, comparisons with data from the literature[1] suggest similar behavior for other regions.

4. EXPERIMENTS

a. Microscopy and Composition

The two samples differ in their mineralogy and texture. Sample A is a poorly sorted, calcareous conglomerate with intraclasts and shell fragment, with extensive development of early carbonate (calcite, dolomite) cements, and later microcrystalline quartz cement. Sample B exhibits a succession of intraclast-bearing, bioturbated medium and fine mudstones. Grains are silt-sized quartz and albite. The matrix is clay rich, with fine microcrystalline quartz cement.

b. Steady State Permeability

Core plugs from the *Wolfcamp* formation from Midland Basin, West Texas were first scanned using a micro-computed tomography (μCT) with a resolution of about 15 μm, eliminating those with any fractures. Plugs were mounted in hydrostatic core holders, thoroughly evacuated, and pressure saturated with toluene. Pressure dependent permeability was measured by increasing the sleeve pressure for fixed pore pressure. The sleeve pressure was changed by applying a mineral oil. The reader is referred to our previous work[1] for detailed description of the experimental setup, and various steps undertaken to ensure complete saturation, dissolution of trapped gas, and avoidance of asphaltene precipitation. Stress creep behavior was observed in these samples, and the measurements were conducted for multiple weeks to ensure steady-state was reached.

c. Nuclear Magnetic Resonance (NMR)

Following the steady state permeability evaluation, the same two core plugs were provided for NMR analysis. They were stress-free for approximately 1 month.

Plugs were mounted in a hydrostatic core holder and placed in the bore of a 2MHz NMR instrument (Maran-2 manufactured by Resonance Instruments). This NMR transparent core holder is equipped with a confining pressure capability (using pressurized NMR-invisible fluorinated fluid FC40) and a flow-through fluid handling system with precision Quizix pumps that control both pore pressure and flow-rate through the core plug. At low

confining pressure of 1,500 psig, toluene was pumped through the core plug, reaching saturation as confirmed by NMR.

The next step was to measure permeability with continuous flow under fixed pore pressure gradient (ΔP). Owing to the low permeability, we found that a high ΔP~1000 psi was necessary. Following this, we equalized pore pressure, ΔP=0, to ensure equal pre-saturation along the core plug for NMR measurements, and simultaneously increased confining and pore pressure to 4,500 psi and 3,500 psi, respectively, to achieve reference toluene saturation at initial NCS of 1,000 psi. Afterwards NCS was step-wise increased through reduction of pore pressure at fixed confining pressure to mimic downhole conditions during oil production. At each stress state, a waiting time of approximately 24 hours was utilized before beginning NMR measurements.

The NMR analysis consisted of T_2 relaxation decay collected using a typical CPMG pulse sequence with inter-echo time of 400 microseconds and repetition delay of 5 seconds. This well-known method provides total amount of fluid in the sample and allows us to separate signal from fluid in different pore or viscosity phases. The NMR signal was rigorously calibrated against several reference samples with a known amount of bulk toluene diluted in NMR-invisible deuterated toluene to fill a similar to core plug magnet volume. Careful calibration is key to measuring fluids for these low-porosity rocks.

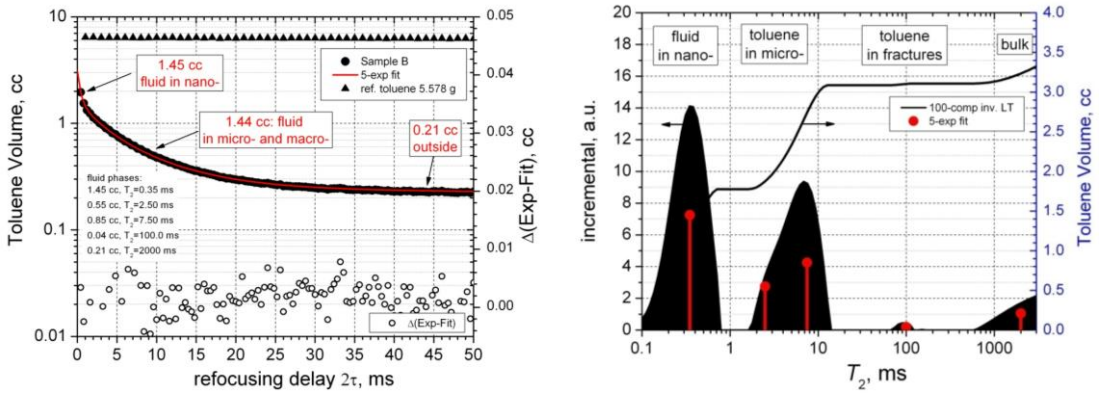

Figure 1. Fluid saturation analysis using NMR measurements: raw NMR signal calibrated against known amount of toluene fitted with sum of five exponential decays (left), inverse Laplace transformation of calibrated NMR signal (right)

Analysis of NMR data was performed by direct fitting raw T_2 relaxation decay curves with a fixed number of exponential decays, usually five, with pre-exponential factors proportional to amount of fluid in a corresponding phase (Fig. 1 left). Determined T_2 values are interpreted as the following fluid phases: fluid in nanopores or heavy hydrocarbons $T_2 < 1$ ms, toluene in micropores 1 ms $< T_2 <$ 20 ms, toluene in macropores and/or fracture 50 ms $< T_2 <$100 ms, bulk toluene outside of core plug $T_2 \sim$ 2400 ms. Although inverse Laplace transformation (LT) provides an appealing visual interpretation of T_2 spectrum (Fig. 1, right). The inverse transformation can be significantly altered by

small changes in a few points. We use inverse LT to guide selection of relaxation times, relying on the amplitudes of the exponential fits to quantify amounts.

d. XMT

Plugs were mounted in a hydrostatic core holder and placed in a specialized liquid/gas feed assembly for use on an XTEK X-ray Tomography device. The X-ray device uses a polychromatic source which irradiates the sample with fan-beam geometry. The source and detector area are fixed and are diametrically opposed on a line going through the cylindrical sample center. Rotation of the sample about its long axis provides the data necessary for 3-D tomographic reconstruction. An important modification to this core holder is a rotary tubing tensioner that allows full rotation of the sample while controlling the confining pressure and pore pressure. With the option of applying ΔP across the sample, this device can measure permeability while simultaneously imaging the in situ fluid movement.

The samples were prepared for analysis by ensuring the pore space was empty. This was typically accomplished through evacuation, although some as-received plugs were also found to be nearly fluid free. Fluid filling was evaluated through NMR analysis.

At the beginning of experiments, a base image of the sample, with empty pores, was made to evaluate the internal structure. Typical 3-D data collection for these would consist of 2500 angle views. Following application of a beam-hardening correction, a standard reconstruction algorithm was applied. Standards inserted in small pits in the sample guide calibration of the linear attenuation coefficients. This results in a 3-D volume image at a native resolution of 30-35 μm per voxel.

Evaluation of the transport in the sample was made through use of an imaging gas. For this, we utilized xenon at elevated pressures. In the pressure range above about 75 psi, xenon exhibits an X-ray attenuation comparable to the mineral matrix.

Imaging time-dependent structures, especially those consisting of both fast and slow regimes, required that we utilize a specialized data collection. For-rapid data collection, we use 2-D data taken at a fixed, “Key Angle”. Here, we rotationally select an end-on view of parallel bedding planes. For longer-times and slow regimes we utilize a locally-created “Sorted Golden Angle” data collection. Small sub-sets of the data (~10 hours) can be utilized for 3-D tomographic reconstruction following long-term structural changes that occur over several days. All data are corrected to place them on an absolute scale, allowing quantitative analysis of linear attenuation.

The stress protocol followed for these samples is as follows: Change the confining stress, wait a fixed time (~ 1 week), measure permeability and image flow, repeat. The fast permeability, perm-streak, is determined through measurement of the pressure decay for an instantaneous xenon gas pressure increase. Imaging of the associated gas movement is made through “Key Angle” data. At later times, we utilize imaging to follow the much slower diffusion of xenon from the high-perm streaks into the matrix.

5. RESULTS AND DISCUSSION

a. Permeability Results and Discussion:

The *Wolfcamp* formation in the Midland Basin of West Texas represents one of the largest hydrocarbon accumulations discovered to date in the United States. According to USGS, the *Wolfcamp* interval contains about 20 billion barrels of oil, 16 trillion cubic feet of associated natural gas, and 1.6 billion barrels of natural gas liquids.[5] The *Wolfcamp* interval is hundreds of feet thick, and has significant variability in terms of in situ pore pressure, mineralogy, clay content, porosity, and total organic carbon (TOC). Quantification of mechanical and flow properties for such heterogeneous interval could provide key inputs in optimal development and depletion of hydrocarbon resources. An example of rock heterogeneity observed in the *Wolfcamp*, is the steady-state liquid permeability for Samples A and B, core plugs from the same well.

Pressure dependent permeability experiments were conducted at two NCS conditions – (1) NCS = 1,500 psi corresponding to in situ NCS and (2) NCS = 5,500 psi corresponding to a drawdown of 4000 psi. The extrapolated steady-state values at higher NCS were normalized using corresponding permeability values at lower NCS. The ratio is plotted in Fig. 2.

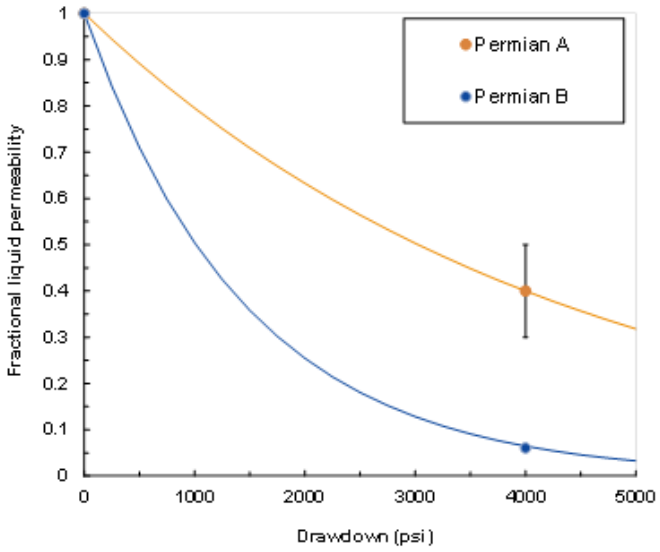

Figure 2. Pressure dependent permeability for two core plugs from *Wolfcamp* are plotted against drawdown assuming the in situ NCS is 1500 psi for this interval. Results here are comparable with those previously published[1], showing a low (Sample A) and high (sample B) stress response. Following that previous work, we describe these responses through use of an exponential function, details of the fit parameters given in the text.

An exponential model provides a good fit to pressure dependent permeability.[1,2] Even though we conducted permeability measurements at only two NCS for these samples, that

experience gave us confidence to use an exponential model. The fractional liquid permeability at an elevated NCS is modeled using the following relationship, and the impairment of permeability is characterized in terms of the permeability exponent "γ."

$$\frac{k}{k_i} = e^{-\gamma(NCS-NCS_i)} \quad (1)$$

where k_i and NCS_i, are respectively the initial permeability and net confining stress.

Sample A (plotted in orange) has lower steady-state permeability ~50 nD at NCS = 1,500 psi, and the permeability declines to ~20 nD at NCS = 5,500 psi. On the contrary, sample B (plotted in blue) has higher permeability of ~990 nD at NCS = 1,500 psi, but the permeability severely declines to ~60 nD at NCS = 5,500 psi. Clearly, sample B displays significantly more pressure dependent permeability than sample A, as shown in Fig. 2. The resulting permeability exponent for sample B is 6.8±0.01 x 10^{-4} /psi, which is significantly higher than the permeability exponent for sample A of 2.3±0.2 x 10^{-4} /psi.

Data reported in our previous publication [1] on *Vaca Muerta* are similar. It is clear that the level of stress dependence is similar for the 2 plugs of Permian *Wolfcamp* to that of the samples from *Vaca Muerta*. However, *Wolfcamp* and *Vaca Muerta* are very different shale plays in terms of location, age, mineralogy, environment of deposition etc. Therefore, such similarity in pressure dependency is surprising.

Motivated by this finding, we utilize various techniques to probe pore-scale changes as a result of increased NCS, in order to explain the reasons behind pressure dependent permeability behavior observed on core plugs.

b. XMT Analysis of Micro-Structure

The images in Fig. 3 were reconstructed from 3-D XMT data collected on the core plugs at ambient pressure. Two cross-sections are shown: one through the mid-plane with the axis of cylindrical sample vertical and a second taken at the mid-point of the sample. The structures are strikingly different. Sample A, exhibits uniform porosity throughout with less severe stress-dependent permeability, and occasional pyrite inclusions, seen as highly-attenuating white blebs in Fig 3. Sample B, in contrast exhibits a strong variation in porosity, focused in planes running parallel to bedding, likely the result of local changes in sorting and particle size. Occasional dark streaks, low-attenuation features, are seen in the vertical cross-section. These features may be filled with low attenuation organic or could be open fissures, but they do not span the sample length. Because X-ray attenuation is calibrated, sub-voxel porosity is indicated by attenuation coefficients less than the mineral matrix. This, combined with in-situ xenon uptake and any subsequent increases in measured voxel attenuation coefficients enables identification of higher porosity regions in the rocks without spatially resolving sub-voxel pore structure.

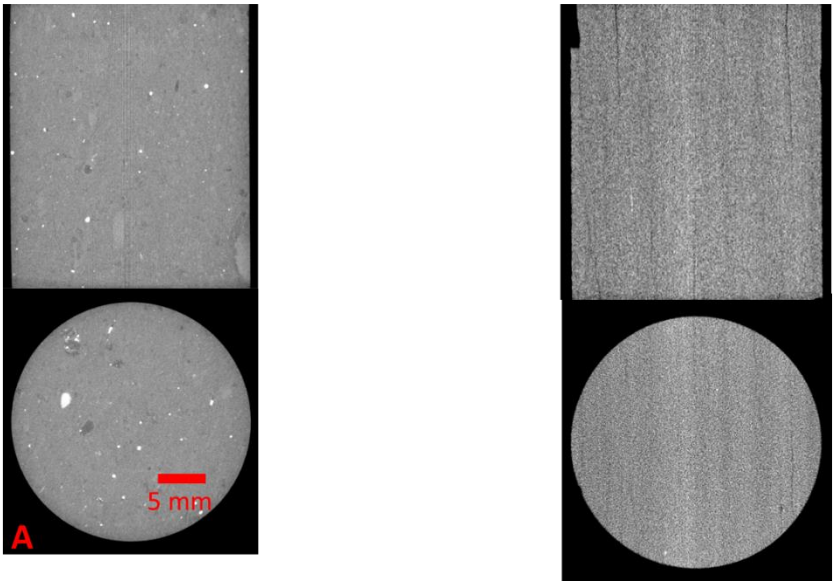

Figure 3. Cross-sections through 3-D reconstruction volumes of Samples A and B. Vertical section along core plug axis, horizontal section at mid plug. The samples are approximately 1 x 1 inch and the resolution of the native images is 30-35 µm per voxel. Sample B exhibits variable-porosity laminae parallel to vertically-oriented bedding planes. These features correlate with high-perm streaks.

c. NMR Analysis of Stress Dependent Pore Structure

Following our protocol, we investigated how the NMR signal responded to changes in NCS. Similar to previous work[6], we find that the overall tendency is for the amount of fluid in the sample to decrease as NCS increases. However, not every pore size is equally affected. As is recognized, tight-oil T_2 spectra can typically be described by a few key relaxation times going from the shortest ~0.1 ms to longest ~2000 ms. Here, we find the relaxation times can be most efficiently described by five exponential decays. The shortest time we attribute to fluid (toluene or water) in nano pores or heavy hydrocarbons [7, 8], the next three are toluene in micro (best fitted by two components suggesting two types of micropores) and macro pores (which may indicate fractures). The longest-T_2 is for bulk toluene in distribution plugs and delivery lines. Signals from the three intermediate components are stress dependent. The changes can be tracked by comparing the calibrated signal level, as expressed by the amplitude of the exponential fit. The relaxation times themselves show little change, T_2 values for fluid in nano- and macro-pores as well as in the bulk do not change while T_2 values of fluid in micropores shows a slight tendency to decrease at higher NCS, suggesting a reduction of micropore size. Our precision in these measurements is enhanced because the core holder is immobile throughout all of the data collection. In addition, a large number of scans were collected, >30,000, resulting in a high signal/noise, >2000. With an approximate fluid volume of 3 cc, this corresponds to a small uncertainty, ~0.0015 cc.

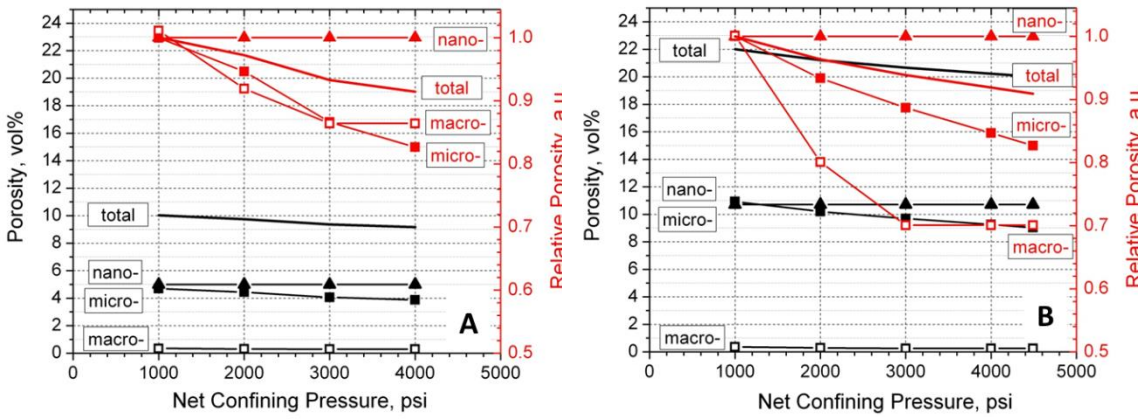

Figure 4. Reduction of total and pore specific fluid filled porosity at increased NCS as measured by NMR on toluene saturated sample A (left) and B (right) expressed in absolute porosity (left axis) and relative porosity (axis) units.

Initial permeabilities measured here are comparable to the initial values, respectively, of 50 nD and 990 nD. We observe reduction of fluid amount in both samples at higher NCS (and confirmed by collection of displaced fluid by Quizix pump), a reduction of pore volume and porosity. Although, the lower porosity sample A is somewhat less compressible, the percent change in total porosity is comparable for both (8% vs. 9%, Fig. 4) with majority of total porosity reduction caused by compression of micropores as they account for approximately half of total porosity. Focusing on behavior of the specific pore systems of higher porosity sample B, we see that the largest percent change is for the macro pores (Fig 4, right), which could include any open fractures as well as the high-perm streaks. While macropore porosity is small (0.34 vol% and 0.36 vol% for samples A and B), the macropore volume decrease by 14% and 30% for samples A and B may be a driver for the strong permeability response. Note how this change occurs over a narrow NCS range of 1,000-3,000 psi and then saturates, perhaps indicating partial closure for high-perm zones. Nevertheless, continuous compression of the micro pores is also observed in both samples and results in approximately 18% reduction of absolute micropore volume, which may also contribute to overall fluid transport through the rock. The component with $T_2 < 1$ ms is the only fluid phase insensitive to NCS. This fluid might be located in either less compressible cemented (nano-) pores of matrix or characterized as a low mobility material (heavy hydrocarbons, bound water, etc.). Given this phase contains approximately half of detected fluid in the rock and might contain valuable hydrocarbons, we continue to study the nature and dynamic behavior of this phase.

d. XMT Analysis of Transport and Structure

Following our protocol, we mounted a companion sample, B2, exhibiting similar structure and porosity to Sample B. NMR evaluation showed the sample pore space was essentially empty. This sample was subjected to 1500 psi confining stress and a full 3-D structure was determined. Layers of high and low porosity were identified, with no visible fractures.

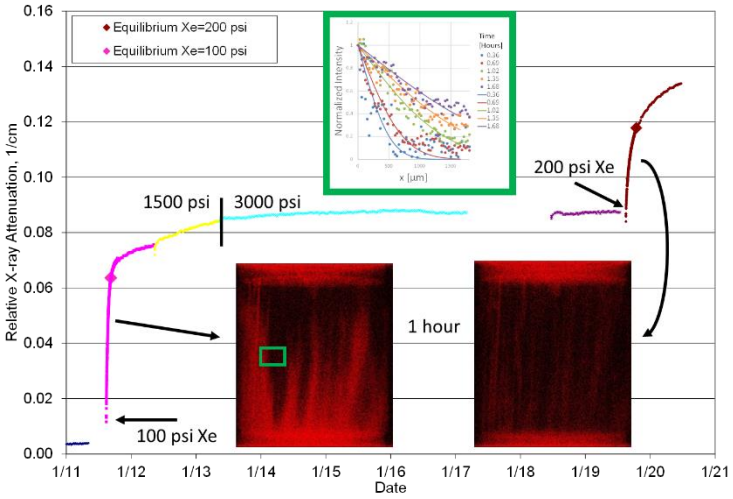

Figure 5 Time transcript of volume-averaged sample attenuation due to xenon flow into the core plug. Data were taken in projection through the cylindrical sample, excluding the porous frits above and below the sample. The individual data points were obtained from image analysis of over 1700 individual frames. Inserts show two of those frames taken one hour after increasing the xenon pressure. Early-time transport is dominated by xenon in high perm zones, and analysis of ΔP yields permeability. Areas adjacent to the high-perm zones fill more slowly. Analysis of xenon concentration, as shown in inset, yields matrix permeability.

The confining stress was maintained at 1500 psi for one week, at which time 100 psi xenon gas was introduced. “Key Angle” scans were initiated prior to gas infusion and by subtracting those initial reference images we obtain a real-time image of the xenon transport. As is clear in Fig. 5, initial transport is concentrated along zones which parallel bedding. The 3-D structure suggests that these high-perm streaks are planar features. After a short time, marked by the solid diamond equilibrium point in the figure, pressure across the sample equilibrates. Further xenon transport is now associated with matrix filling and this proceeds much more slowly. We followed a similar protocol for 3000 psi confining stress. During the 1 week waiting period, the sample attenuation (a measure of xenon content), seems to decline very slightly. 3-D data were reconstructed into 3-D volumes and analyzed for strain, but it was below our detection limit of 2×10^{-3}. At the end of this period, the xenon gas pressure was again increased (to 200 psi), difference images for “Key Angles” (obtained by subtracting reference images at 100 psi) show similar high-perm streaks as at lower stress. This is significant, since we would have expected open fractures to have closed by 3000 psi confining stress.[2] Pressure equilibration occurs rapidly (minutes) followed by slower (hours) matrix filling.

Using conventional pressure jump analysis, we obtain the early-stage sample permeability. Utilizing transport equations for a compressible gas flowing from a fixed upper pressure into a bottom reference volume (several times larger than the pore volume), we obtain the sample permeability. Evaluating the Klinkenberg correction for xenon is problematic, as there are no reported values for the constant, *b*. Here we used the

N_2 values modified slightly to account for the difference in mean free path between the two molecules. The values applied are *b*= 100 and 200 psi for 1500 and 3000 psi confining stress. At NCS= 1400 and 2800, permeabilities are 15000±1000 and 3500±500 nD. These values are higher than for sample B, but with transport controlled by the high-perm streaks, it is most likely they are present at a slightly higher density of such features in sample B2. The decline in permeability with NCS is similar for both toluene and xenon transport.

To measure matrix transport we employ the linear relationship between X-ray attenuation and xenon concentration. Careful attention to data collection and processing ensures that the attenuation data are all referenced to a common baseline. We can then use the spatially-resolved change in attenuation with time to measure local xenon concentration. Concentration profiles are analyzed using an assumption of diffusion from a planar source of constant concentration. An example is shown in Fig. 5, with a typical value for diffusion of D=1 x 10^{-6} cm^2/s. To calculate the matrix permeability we utilize the familiar pressure diffusion equation $= D\mu/B$, where the bulk modulus *B* for a gas is simply the pressure and the viscosity, μ= 2.3 x10^{-5} Pa s, from NIST[9]. At NCS= 1400 and 2800 psi, the resulting permeability values are k= 0.81±0.6 and 0.78±0.6 nD. Consistent with expectations, these are considerably smaller than the perm-streak values, and they show no significant variation with stress. We also analyzed the volume-averaged sample attenuation, obtaining similar values.

6. SUMMARY

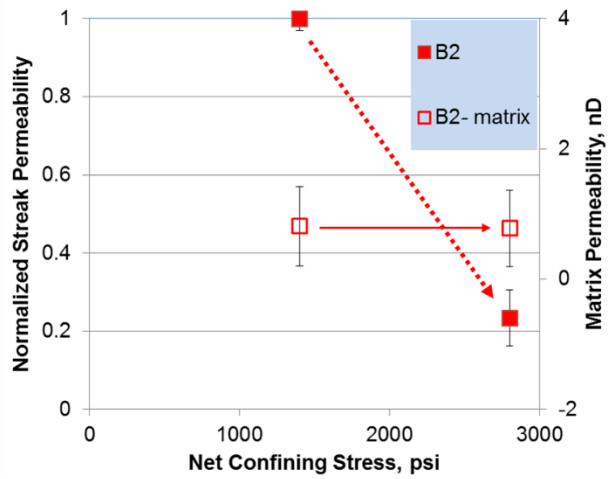

Figure 6. Summary of transport measured via XMT analysis. Solid symbols, showing significant stress dependence, are permeability values associated with perm-streaks The open symbols are for matrix permeability and show no stress response within experimental uncertainty.

The results here show that with changing NCS the NMR-measured micro and macro porosities change, whereas nano porosity is unchanging. We acknowledge that artifacts can be introduced based on workflow (steady-state perm -> NMR -> microCT), and

irreversible hysteresis. There may have been material changes in the microstructure during coring/ surfacing/ handling operations. However, if only the matrix permeability is intrinsic to the rock, our results suggest no stress dependent permeability would occur. We compare those observations to the XMT results showing that perm-streak permeability is affected by changing NCS but not that of the matrix. Transport is highly sensitive to pore-throat changes. With no changes for matrix transport nor for NMR nano porosity, these quantities appear arise from the same structures. This same logic implies that both the NMR micro and macro pores are part of the high perm streak. XMT data support this conclusion. Fig. 5 shows that comparison of the linear attenuation change before equilibrium (perm streak) with that afterwards (matrix) suggests that about 75% of the volume is in the perm-streaks with the remainder in the matrix. NMR analysis is in rough agreement, with about 50% of the volume in micro plus macro pores. With the permeability so strongly affected in Sample B, and an associated sharp change in NMR macro porosity, it is likely those pores which control permeability.

Others have suggested that stress dependent permeability arises from compression of high-perm regions, for example Rydzy et al.[2]. Their analysis found a similar power law behavior for permeability vs. NCS, as first reported by Chhatre et al. [1]. However Rydzy et al. attributed this to fracture closure, with fractures being a probable artifact of exhumation of the core plug.. In conventional rocks, fracture closure effects on permeability are well known. There, permeability of the matrix is investigated by first applying sufficient stress to close fractures.[10] As expected for a stiff rock matrix with an open aperture, fracture closure occurs at low stress, and this leads to a substantial change in permeability[11, 12]. Afterwards the intrinsic matrix permeability is observed. The circumstances for tight oil samples seem distinctly different. The stresses required to alter the permeability are considerably higher. Also, there is a distinct ductile strain component, evident in the long times to reach equilibrium for steady-state permeability. Finally, the high-stress permeability remains larger than the matrix permeability. This suggests a more complex strain phenomena.

7. CONCLUSIONS

- Pressure dependent perm can be characterized accurately
- NMR studies indicate
    - Three distinct grouping of the peaks in the T_2 spectra which are speculated to represent nano, micro and macro pores
    - The three kinds of porosity have different response to increases NCS
- XMT studies indicate the differences between the two Permian samples in terms of the presence of high perm streaks
    - Effective transport properties along and perpendicular to the streaks can be calculated using diffusion of Xenon
    - Response of transport properties with increasing stress is different for the streaks vs inherent matrix

8. ACKNOWLEDGEMENTS

Discussions and assistance with permeability from Deniz Ertas, ExxonMobil Research & Engineering Company are gratefully acknowledged.

9. REFERENCES

1. Chhatre, S.S., et al., *Steady-State Stress-Dependent Permeability Measurements of Tight Oil-Bearing Rocks.* Petrophysics, 2015. **56**(02): p. 116-124.
2. Rydzy, M.B., et al. *Stressed Permeability in Shales: Effects of matrix compressibility ad fractures – A step towards measuring matrix permeability in fractured shale samples*. in *International Symposium of the Society of Core Analysts*. 2016. Snowmass, CO.
3. Martin, J.A.Q. and D. Devegowda. *Modeling-Based Recommendations for Drawdown Management in Liquids-Rich Shale Wells*. 2015. Unconventional Resources Technology Conference (URTEC).
4. Devegowda, D. *Modelling Based Recommendation for Choke Management in Shale Wells*. in *Unconventional Resources Technology Conference*. 2015. Society of Petroleum Engineers.
5. USGS. *https://www.usgs.gov/news/usgs-estimates-20-billion-barrels-oil-texas-wolfcamp-shale-formation*. 2016.
6. Dick, M., et al. *Understanding Fractures and Pore Compressibility of Shales using NMR*. in *Internatonal Symposium of the Society of Core Analysts*. 2016. Snowmass, CO.
7. Kausik, R., et al., *NMR relaxometry in shale and implications for logging.* Petrophysics, 2016. **57**(04): p. 339-350.
8. Washburn, K.E. and J.E. Birdwell, *Updated methodology for nuclear magnetic resonance characterization of shales.* Journal of Magnetic Resonance, 2013. **233**: p. 17-28.
9. Lemmon, E., M. McLinden, and D. Friend, *Thermophysical Properties of Fluid Systems*, in *NIST Chemistry WebBook, NIST Standard Reference Database Number 69*, P. Linstrom and W. Mallard, Editors. 2015, National Institute of Standards and Technology: Gaithersburg MD.
10. Zhu, W. and T.f. Wong, *The transition from brittle faulting to cataclastic flow: Permeability evolution.* Journal of Geophysical Research: Solid Earth, 1997. **102**(B2): p. 3027-3041.
11. Brace, W.F., J. Walsh, and W. Frangos, *Permeability of granite under high pressure.* Journal of Geophysical research, 1968. **73**(6): p. 2225-2236.
12. Pyrak-Nolte, L. and J. Morris, *Single fractures under normal stress: The relation between fracture specific stiffness and fluid flow.* International Journal of Rock Mechanics and Mining Sciences, 2000. **37**(1): p. 245-262.